Wing-Body Interference Lift for Supersonic Missiles with Elliptical Cross-Section Fuselages

H. F. Nelson*
University of Missouri—Rolla, Rolla, Missouri

The effect of elliptical fuselage cross sections on wing lift is calculated for supersonic, delta-wing missiles at Mach 3 and 4. Aspect ratios of 2.4, 3.2, and 4.0 are considered. Wing lift in the presence of an elliptical fuselage is computed by solving the Euler equations using a finite-difference method, and it is presented in terms of the wing-body interference parameter $K_{W(B)}$. The fuselage cross sections are defined in terms of the ratio of their vertical-to-horizontal semiaxes B/R. $K_{W(B)}$ values are presented for $B/R = 0.33$, 0.50, 0.75, 1.0, 1.5, 2.0, and 2.4 for planar and cruciform fin configurations. Numerical results at constant Mach number and fin size show that $K_{W(B)}$ decreases as B/R increases. For small fins, typical of missiles, wing lift is quite sensitive to fuselage shape; whereas for large wings, typical of airplanes, wing lift is not very sensitive to fuselage shape. As Mach number increases for a specific fin size, $K_{W(B)}$ increases slightly for $B/R < 1$ and decreases slightly for $B/R > 1$; however, for preliminary design purposes the change in $K_{W(B)}$ with Mach number is negligible. Evaluation of $K_{W(B)}$ is necessary for missile preliminary design component build-up methods. Simple equations are presented for $K_{W(B)}$ as a function of wing span to body radius ratio and B/R, which are suitable for preliminary design. $K_{W(B)}$ values from this research are the only ones available for elliptical cross section fuselages.

Nomenclature

A_W = planform area of wing formed by joining two fins
AR = aspect ratio of wing formed by joining two fins
B = vertical semiaxis of missile body (at $\phi = 0$ deg)
B/R = ratio of vertical semiaxis to horizontal semiaxis for missile body
$K_{W(B)}$ = wing-body interference factor due to upwash
K_ϕ = fin–fin interference factor due to sideslip
L_W = lift on wing alone
$L_{W(B)}$ = lift on wing in the presence of body
M = Mach number
q_∞ = dynamic pressure
r = local radius of missile fuselage
R = horizontal semiaxis of missile body (at $\phi = 90$ deg)
S = fin span, measured from body centerline
S/R = fin span/body radius ratio
V = velocity
V_c = crossflow velocity far from body
V_∞ = missile velocity
Z = missile axial coordinate measured from nose
Z_c = axial location of end of nose
Z_n = axial location of end of conical nosetip
Z_w = wing axial location on missile
α = missile angle of attack
α_{eq} = equivalent angle of attack
α_F = fin angle of attack
β_F = fin sideslip angle
ε = wing semivertex angle
ϕ = angular coordinate measured from bottom of fuselage
$(\Delta\alpha_{eq})_v$ = induced change in angle of attack due to vortices

Introduction

ACCURATE and fast prediction of missile aerodynamic force and moment characteristics for various combinations of fin geometries and body cross-sectional shapes is necessary in preliminary design tradeoff studies. Aerodynamic interference between adjacent surfaces of missiles can have large effects on the performance of a particular configuration. Evaluation of these interference effects (sometimes called "carryover factors") presents a challenge to the preliminary designer. Wing-body interference for circular fuselage cross sections has been intensely investigated[1–12]; however, only limited examinations of elliptical body cross sections have been performed.[13–16]

Allen and Pittman[13] published a study of computational methods for analysis of missile body shapes with elliptical cross sections up to 1984. They mainly compared two numerical codes, developed prior to SWINT,[9,10,17] with experimental surface pressure and normal force data. Neither code adequately calculated separated-flow nonlinearities on the leeward surface and attached-flow nonlinearities on the windward surface.

Amidon[14] measured surface pressure on advanced missile bodies with elliptical cross sections in supersonic flow. Models with ellipticity ratios of 2:1, 2.5:1, and 3:1 were tested at Mach numbers from 1.5–5.0 and angles of attack from 0–20 deg. The data were compared to numerical predictions from several codes including SWINT ("NSWC code" in Ref. 14). The SWINT code accurately predicted the circumferential pressure-coefficient variation. This good agreement with experimental data indicates the potential of SWINT to predict elliptic body aerodynamics. Codes prior to SWINT could not accurately predict the aerodynamic characteristics of elliptical cross-sectional bodies.[13]

Allen and Townsend[15] presented and analyzed pressure and force predictions obtained using SWINT. They investigated a variety of configurations ranging from simple axisymmetric bodies to complex bodies with wings, tails, and inlets at low supersonic to low hypersonic Mach numbers. SWINT predicted accurate results for axisymmetric bodies with attached flow; however, leeside accuracy was poor due to the modeling of flow separation in the code.

Priolo and Wardlaw[16] applied the ZEUS numerical code to missiles with noncircular fuselage cross sections. ZEUS is based on solving the Riemann problem for steady, supersonic flow and it is cast in a control volume form rather than a finite-difference form. Surface pressure, normal force, and pitching moment results from ZEUS agreed well with experi-

Received Nov. 17, 1988; revision received Feb. 18, 1989.

*Professor, Aerospace Engineering, Thermal Radiative Transfer Group, Department of Mechanical and Aerospace Engineering. Associate Fellow AIAA.

ment for bodies alone and body-wing-tail configurations with elliptical cross sections without the use of artificial viscosity or other special procedures.

Equivalent Angle-of-Attack Method

Component-buildup methods yield fast and economical ways of evaluating fundamental preliminary design parameters such as force and moment coefficients and stability derivatives. A specific component-buildup method used to evaluate forces on missile fins is called the equivalent angle-of-attack method. It models the nonlinear lifting characteristics of missile fins in terms of an equivalent angle of attack[18]

$$\alpha_{eq} = K_{W(B)}\alpha_F + \frac{4}{AR} K_\phi \alpha_F \beta_F + (\Delta\alpha_{eq})_v \qquad (1)$$

The terms on the right-hand side of Eq. (1) represent contributions due to body upwash, fin sideslip angle, and vortex interaction, respectively. The equivalent angle-of-attack method is developed and its accuracy is demonstrated in Ref. 18. Extension of the method to high angles of attack is discussed in Refs. 19–21.

Vukelich[22] described a process for the aerodynamic design of elliptically shaped cross section missile configurations using component-buildup methods. The process can be applied to elliptical cross section bodies, winged elliptical bodies, and elliptical bodies with multiple lifting surfaces. He presents preliminary design data for normal force, pitching moment, and center of pressure over a wide range of Mach numbers (0.5–1.6) and angle of attack (0–60 deg).

The objective of this research is to determine the wing-body interference due to upwash, $K_{W(B)}$, for missiles with elliptical cross section fuselages. $K_{W(B)}$ is defined as the lift on the wing in the presence of the body divided by the lift on the wing alone:

$$K_{W(B)} = \frac{L_{W(B)}}{L_W} \qquad (2)$$

When $K_{W(B)} > 1$, the body produces positive lift interference and the fin-body combination produces more lift than the fin alone. If $K_{W(B)} < 1$, the body reduces the lift on the fin compared to the fin-alone case.

The evaluation of K_ϕ is presented in Refs. 5, 11, and 12 for missiles with circular cross-section fuselages. The effect of $(\Delta\alpha_{eq})_v$ is negligible for small angles of attack.

Analysis

Flowfield

The SWINT numerical code was used for this research.[17] SWINT uses a finite-difference axial marching scheme to solve the Euler equations in supersonic flow domain bounded by the body and the bow shock. The fins are modeled as discontinuities in the solution domain using a thin-fin approximation. The conservation equations are cast in conservative form allowing shock waves to be captured by the numerical scheme. Exact boundary conditions are used wherever possible; however, empirical boundary conditions are necessary when phenomena such as subsonic fin leading edges or body-wing root junctions are encountered. The computation is started by specifying an initial data plane near the nose of the missile. The flowfield solution is advanced by marching axially along the missile body. SWINT predictions generally agree well with both experimental data and other numerical results for a wide variety of missile configurations and flight conditions.[10–12]

Wing-Alone Lift

$K_{W(B)}$ is determined by normalizing $L_{W(B)}$ with the wing-alone normal force as shown in Eq. (2). Ideally, SWINT would be used to determine L_W by computing the normal force on a wing composed of two fins joined together at their root chords. However, SWINT requires that the fins lie entirely within the missile bow shock; therefore, a wing-alone case cannot be analyzed. Linearized potential theory was used to determine L_W.[12] For a fin alone with supersonic edges, L_W is

$$L_W = 4\alpha_F q_\infty A_W/(M^2-1)^{1/2} \qquad (3)$$

Equation (3) was used to determine L_W for all of the cases reported herein, since fins with subsonic leading edges are not considered.

Missiles with fin span/body radius ratios S/R up to 20 were analyzed using SWINT to check SWINT predictions against linearized potential theory in Ref. 12. As the fins became large relative to the body, $L_{W(B)}$ predicted by SWINT asymptotically approached L_W predicted by linearized potential theory. L_W as predicted by Eq. (3) was also checked against values predicted using Missile Datcom methods.[23] The agreement was within 2% for the range of parameters considered herein. Thus, the use of Eq. (3) to determine L_W is justified.

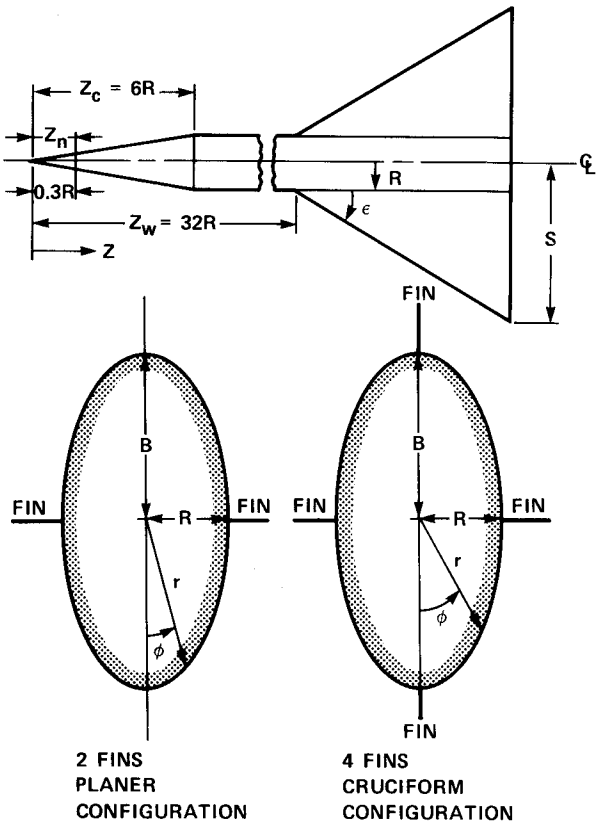

Fig. 1 Missile geometry and nomenclature.

Missile Geometry

This research evaluates $K_{W(B)}$ as a function of wing span/body radius S/R, for missiles with elliptical fuselage cross sections as shown schematically in Fig. 1. The fuselage cross sections are characterized by the ratio of their vertical to horizontal dimensions, B/R. The fins were infinitely thin flat plates with triangular planforms. Missile configurations with two and four fins oriented symmetrically around the fuselage, such that one set of fins was always horizontal as shown in Fig. 1, were considered. The horizontal fin at $\phi = 90$ deg was used for the $K_{W(B)}$ analysis because $\alpha_F = \alpha$ for this fin. The fin aspect ratio is an important correlation parameter. For a delta wing, it is defined as

$$AR = \frac{(2S)^2}{A_W} = 4\tan\varepsilon \qquad (4)$$

where A_W is the planform area of the wing.

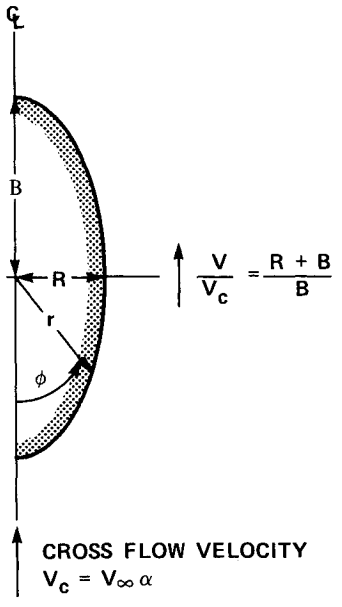

Fig. 2 Crossflow velocity on missile fuselage.

The missile fuselage consisted of a linearly tapered, elliptical cross-section nose cone and an elliptical cross-section cylindrical body. For the straight-sided body ($Z > Z_c$), the radius was given by

$$r = BR/(R^2\cos^2\phi + B^2\sin^2\phi)^{1/2} \tag{5}$$

For the linearly tapered nose cone ($0 \le Z \le Z_c$), the radius was obtained by multiplying Eq. (5) by Z/Z_c, where $Z_c = 6R$.

The numerical starting solution would not converge for the linearly tapered elliptical nose cones for missile bodies with vertical to horizontal semiaxis ratios (B/R) of 0.50 and 0.33. Thus, a conical nose tip, such that $r = RZ/Z_c$, was used for $0 < Z < Z_n$ to start the solution. Z_n was taken to be $0.3R$. Thus, the radius of the circular cone at $Z = Z_n$ was $0.05R$. A conical shape that varied linearly from a circle at $Z = Z_n = 0.3R$ to an ellipse at $Z = Z_c = 6R$ was used for the missile nose between Z_n and Z_c. Therefore, for $Z_n \le Z \le Z_c$ the nose radius was

$$r = [r_e(Z - Z_n) + r_c(Z_c - Z)]/[Z_c - Z_n] \tag{6}$$

where r_e is the radius of the ellipse given by Eq. (5) and r_c is the radius of the circular nose tip at $Z = Z_n$ ($r_c = 0.05R$). Numerical results for the fin forces using this nose shape were compared to those calculated using the linearly tapered elliptical nose for $B/R = 0.75$ and 1.50 and were found to be the same.

The elliptical cross sections investigated were $B/R = 0.33$, 0.50, 0.75, 1.0, 1.5, 2.0, and 2.4. The leading edge of the root chord of the delta wing began at $Z = Z_w = 32R$. Thus, it was far enough downstream to minimize the influence of the nose shape on the wing lift, primarily due to the expansion wave from the junction of the nose and the missile body. Only one-half of the missile ($0 \text{ deg} \le \phi \le 180 \text{ deg}$) was analyzed because the flowfield was symmetrical about the B-plane.

Limiting Values of $K_{W(B)}$

In the limit when S/R approaches 1, the value of $K_{W(B)}$ is hard to calculate numerically because the number of grid points on the fin becomes small. However, in this limit linearized potential theory can be applied, because as the fins become small relative to the body they do not interact with each other.

For small angles of attack, linearized potential theory predicts the crossflow velocity components for flow around an ellipse.[24-26] Following Refs. 24–26, the crossflow velocity on the ellipse shown in Fig. 2 at $\phi = 90$ deg is

$$V = V_c(R + B)/B \tag{7}$$

in terms of the ellipse geometry, where $V_c = V_\infty \alpha$ for small angles of attack. For an infinitely small wing located on the missile centerline, the flow over the wing is the same as the flow on the body at $\phi = 90$ deg and $r = R$. Thus, the increase in the velocity around the missile body effectively increases the angle of attack on the small wing by the factor $(R + B)/B$ compared to the wing alone. This yields

$$K_{W(B)} = (R + B)/B \tag{8}$$

at $S/R = 1$. For a circular cross-section fuselage, $B = R$, and $K_{W(B)}$ goes to 2 for very small fins. In the limit, when B becomes very large with respect to R, the fuselage cross section approaches a vertical flat plate of negligible thickness and $K_{W(B)}$ goes to 1. Physically, this limit is equivalent to the case of S/R going to infinity for a finite-span fin. For this situation, $K_{W(B)}$ goes to 1 because the fuselage becomes infinitely small and its interference effects on the fin become negligible.

Table 1 Numerical grid size along the missile body for each B/R value (number of r planes × number of ϕ planes)

B/R	$Z/R \le 10$	$10 \le Z/R \le 20$	$20 \le Z/R \le 30$	$Z/R \ge 30$
0.33 ($M = 3$)	30 × 40	60 × 60	70 × 70	120 × 81
0.33 ($M = 4$)	30 × 40	40 × 60	60 × 80	120 × 81
0.50	30 × 40	40 × 60	50 × 70	120 × 81
0.75	20 × 20	40 × 35	60 × 50	72 × 61
1.00	20 × 20	40 × 35	60 × 50	72 × 61
1.50	20 × 20	40 × 35	60 × 50	120 × 81
2.00	20 × 20	40 × 35	60 × 50	120 × 81
2.40	30 × 30	45 × 50	60 × 70	120 × 81

Results and Discussion

Numerical Considerations

SWINT results for $L_{W(B)}$ were determined using a finite-difference grid that was uniformly distributed between the body and the bow shock. It was necessary to decrease the grid size as B/R increased above 1 or decreased below 1 to keep enough points in the high-curvature regions of the flowfield for accurate calculations. The grid size was also changed at several axial stations as the calculation marched along the fuselage in order to maintain accuracy and optimize computer time. The grid was made progressively smaller by trial and error until the $L_{W(B)}$ values converged. A finer grid was used for $B/R = 0.33$, 0.50, and 2.4 at $Z/R \le 10$ to improve the flowfield calculations over the nose and to reduce the effects of possible nose flowfield inaccuracies further downstream. SWINT was unable to start a solution with an initial grid of 20×20 (r planes × ϕ planes) for $B/R = 2.4$, because of the relatively small local radius of curvature of the body cross section near $\phi = 0$ and 180 deg. This grid did not put enough points in the high-curvature regions to define the rapid turning of the crossflow on the body. The same problem occurred to an even greater extent for $B/R \le 0.75$ near $\phi = 90$ deg. Table 1 presents a complete summary of the gridding used in the calculations.

Numerical accuracy was hard to maintain for S/R less than 2.0, because of the low number of grid points on the small fins. For these cases, the fin span was small compared to the radial distance between the body and the bow shock. The calculations were done with evenly spaced grid points between the body and the bow shock. (SWINT has the capability of

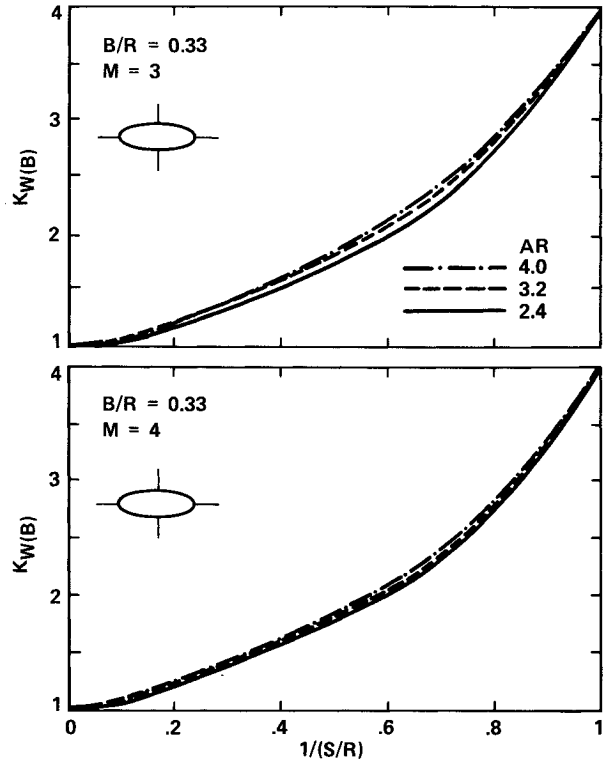

Fig. 3 $K_{W(B)}$ as a function of $1/(S/R)$ for $B/R = 0.33$ at aspect ratios of 2.4, 3.2, and 4.0. Upper graph at Mach 3; lower graph at Mach 4.

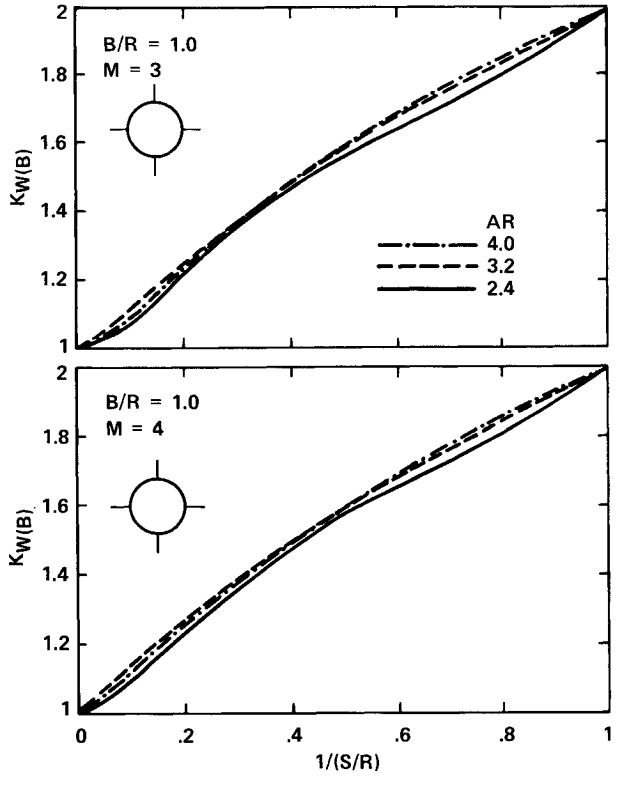

Fig. 4 $K_{W(B)}$ as a function of $1/(S/R)$ for $B/R = 1.0$ at aspect ratios of 2.4, 3.2, and 4.0. Upper graph at Mach 3; lower graph at Mach 4.

using a nonuniform grid, but it is complicated to use.) This leads to a relatively small number of grid points that fall on the fin, which reduces the accuracy of the normal force calculation. In addition, SWINT employs an empirical correlation to handle the body-wing root junction. This leads to additional error, which is significant for small fins. The numerical inaccuracies at small S/R were overcome by fairing in

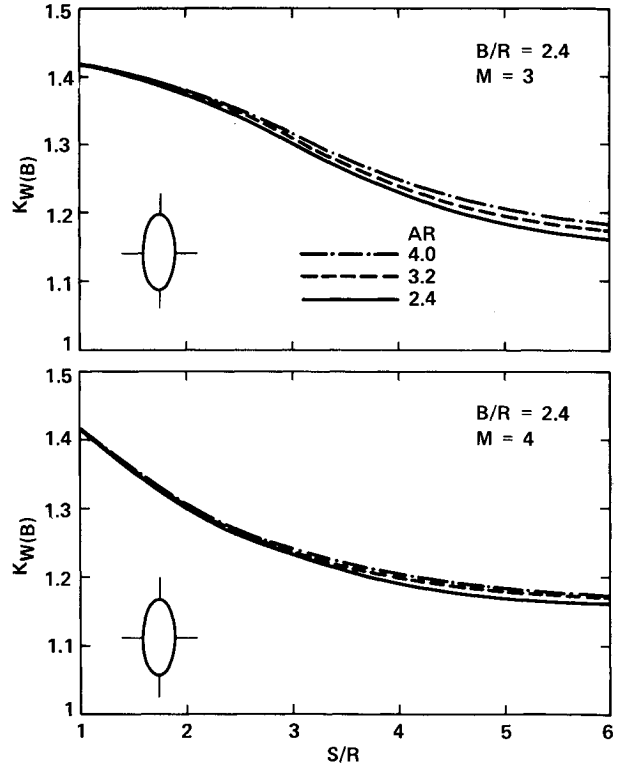

Fig. 5 $K_{W(B)}$ as a function of S/R for $B/R = 2.4$ at aspect ratios of 2.4, 3.2, and 4.0. Upper graph at Mach 3; lower graph at Mach 4.

a smooth curve from the limiting value of $K_{W(B)}$ at $S/R = 1$ [given by Eq. (8)] to the value of $K_{W(B)}$ calculated from SWINT at the smallest S/R value for which the SWINT predictions were accurate ($S/R \sim 1.75$). Also, for the figures that show $K_{W(B)}$ vs $1/(S/R)$, the curves are faired in for $0 \leq 1/(S/R) < 0.167$ because $K_{W(B)}$ goes to 1 as S/R approaches infinity for planar and cruciform fin configurations.

Flight Conditions

Four flight conditions ($M = 3$, 4 and $\alpha = 2$, 3 deg) and three delta-wing planforms ($AR = 2.4$, 3.2, 4.0, or $\varepsilon = 30.964$, 38.66, 45.0 deg) were examined to determine the effect of M, α, and AR on $K_{W(B)}$ for specific values of B/R from 0.33–2.4. The effect of angle of attack turned out to be negligible, as expected, for small angles of attack where the forces are linear with α. Angle-of-attack effects will become important at larger values of α.

Aspect Ratio

Typical variation of $K_{W(B)}$ with respect to S/R for B/R values of 0.33, 1.0 and 2.4 are shown in Figs. 3–5 for aspect ratios of 2.4, 3.2, and 4.0. Note that $K_{W(B)}$ is shown vs $1/(S/R)$ in Figs. 3 and 4 and that it is plotted vs S/R in Fig. 5. Each figure shows data for Mach 3 and Mach 4 for $1 \leq S/R \leq 6$. The intercept at $S/R = 1$ is the predicted $K_{W(B)}$ value from Eq. (8). $K_{W(B)}$ values greater than 1 indicate positive contribution to wing-body lift with respect to the wing alone due to the presence of the body.

Figures 3–5 show that $K_{W(B)}$ is largest for small values of S/R (typical of missiles). This indicates larger positive effects on wing lift due to the presence of the fuselage at small values of S/R. For large values of S/R (typical of airplanes), $K_{W(B)}$ approaches one and the effect of the fuselage on the wing lift becomes negligible. In addition, the effect of the fuselage shape is significant, especially for small values of S/R (missile configurations). Low, wide fuselages increase the value of $K_{W(B)}$ at small S/R much more than high, narrow fuselages. This trend is reasonable, because when B/R becomes very large the fuselage becomes an infinitely thin, vertical flat plate.

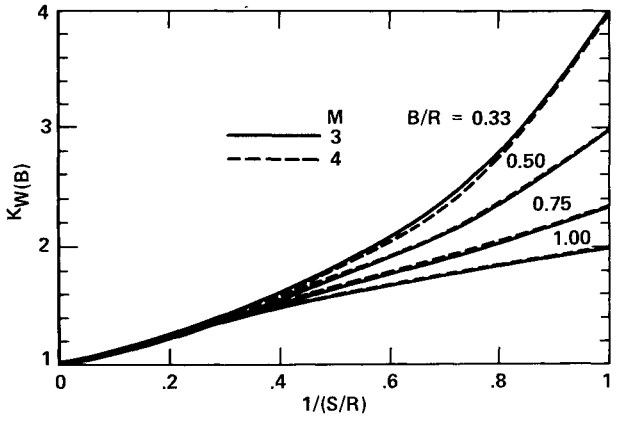

Fig. 6 Effect of Mach number on $K_{W(B)}$ for $B/R = 0.33$, 0.50, 0.75, and 1.0.

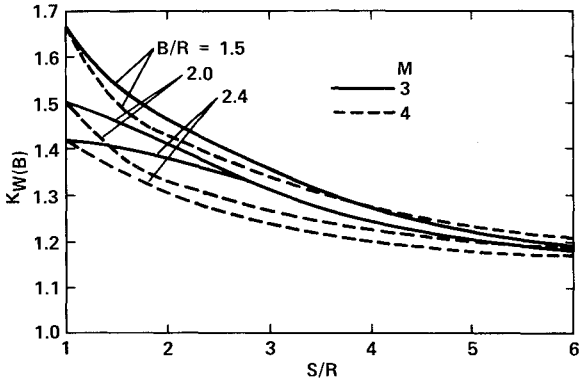

Fig. 7 Effect of Mach number on $K_{W(B)}$ for $B/R = 1.5$, 2.0, and 2.4.

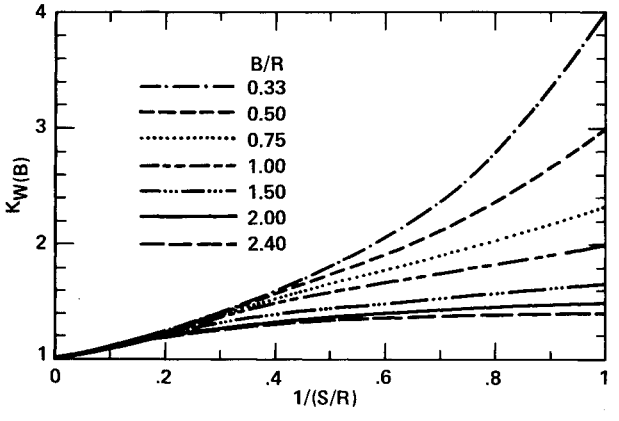

Fig. 8 Preliminary design values of $K_{W(B)}$ vs $1/(S/R)$.

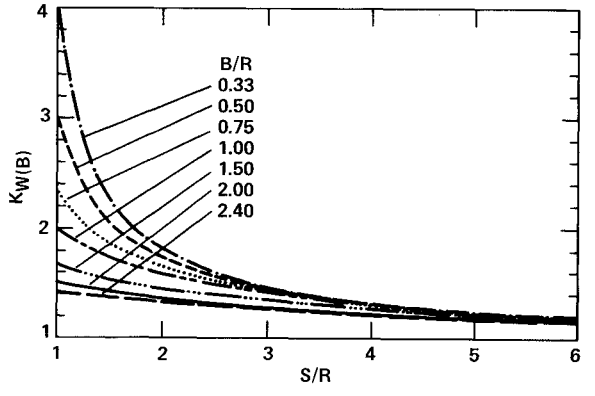

Fig. 9 Preliminary design values of $K_{W(B)}$ vs S/R.

Hence, the velocity and pressure fields are not affected by the fuselage, because the crossflow is nonviscous and at zero angle of attack. Consequently, in this limit $K_{W(B)}$ approaches 1 for all values of S/R. In the opposite limit, when B/R goes to zero, the fuselage becomes very wide and its height goes to zero. The fuselage becomes an extension of the wing. In this case, the crossflow impinges on the bottom of the fuselage and does not flow around it. There is essentially no crossflow velocity above the fuselage because of the strong blockage and this makes $K_{W(B)}$ very large, especially for fins with S/R values near 1. This limit roughly represents the blended wing and it has a large positive interference lift.

In general, the effect of changing aspect ratio on $K_{W(B)}$ is insignificant over the range of parameters shown. Thus, the data can be averaged over aspect ratio for use in component-buildup methods. This eliminates aspect ratio as a first-order parameter in preliminary design.

Mach Number

The effect of changing M from 3 to 4 on $K_{W(B)}$ is shown in Figs. 6 and 7 as a function of S/R for $AR = 3.2$. Figure 6 shows data for $B/R = 0.33$, 0.50, 0.75, and 1.0; and Fig. 7 shows data for $B/R = 1.5$, 2.0, and 2.4. At a given value of S/R, $K_{W(B)}$ at Mach 4 is greater than $K_{W(B)}$ at Mach 3 if $B/R < 1$; however, if $B/R > 1$ the opposite is true. The value of $K_{W(B)}$ is insensitive to Mach number for $B/R \leq 1$; however, for $B/R > 1$, $K_{W(B)}$ changes slightly with Mach number. The sensitivity to Mach number is partially magnified because of the scales for $K_{W(B)}$ on the two figures.

Preliminary Design

The sensitivity of $K_{W(B)}$ to changes in the basic parameters is somewhat uncertain because the calculations were based on the Euler equations, and hence neglected the effects of boundary layers and possible flow separation. To the first-order, $K_{W(B)}$ is mainly dependent on S/R and B/R. Thus, the $K_{W(B)}$ data can be averaged over Mach number and aspect ratio for use in preliminary design. Figure 8 shows the $K_{W(B)}$ as a function of $1/(S/R)$, whereas Fig. 9 shows the same data vs S/R. The data shown in Figs. 8 and 9 was obtained by averaging the SWINT $K_{W(B)}$ data over angle of attack, aspect ratio, and Mach number. This yields one curve for $K_{W(B)}$ as a function of S/R for each value of B/R. Table 2 presents numerical values for $K_{W(B)}$ as a function of S/R for the B/R ratios used in this research. Equations for $K_{W(B)}$ as a function of S/R, which are suitable for preliminary design, are presented in the Appendix. Table 2 was generated using these equations, and the values of $K_{W(B)}$ presented are valid for supersonic flow at low angles of attack.

Comparison with SBT and Experiment

Figure 10 presents a comparison of the present numerical Euler code $K_{W(B)}$ results (SWINT) with both slender body theory (SBT)[1] and experiment.[27] The curve labeled SWINT is the preliminary design data for $K_{W(B)}$ for a circular cross-section fuselage ($B/R = 1$) as listed in Table 2. SWINT predicts larger values of $K_{W(B)}$ than the slender body theory analytical solution. This implies a larger, positive fin-body interference. The SWINT $K_{W(B)}$ values should be more accurate than the SBT values because SWINT accounts for vorticity and shock waves, whereas SBT ignores these effects.

The experimental points on Fig. 10 are derived from the Tri-Service-NASA data base.[27] This data base was developed from a large series of tests carried out by the NASA Langley Research Center.[28] The experimental data applicable to the current research is at $S/R = 2$, $AR = 2$, and $\alpha = 2.5$ and 5 deg for $M = 2.5$, 3.5, and 4.5. The $K_{W(B)}$ values from Table 4 of Ref. 27 for fins with supersonic edges are presented in Fig. 10. The experimental data for $K_{W(B)}$ is generally in the range from 1.40–1.53 with one point at 1.19 ($M = 4.5$ and $\alpha = 5$ deg). The low experimental value may be due to the formation of vortices along the fin leading edge and the difference in fin

Table 2 Preliminary design values for $K_{W(B)}$ for $2 \le M \le 4$ and $\alpha \le 5$ deg

	B/R						
S/R	0.33	0.50	0.75	1.00	1.50	2.00	2.40
1.00	4.000	3.000	2.333	2.000	1.667	1.500	1.417
1.20	2.962	2.460	2.089	1.865	1.597	1.466	1.400
1.40	2.419	2.153	1.927	1.768	1.541	1.436	1.384
1.60	2.122	1.965	1.812	1.695	1.498	1.410	1.369
1.80	1.945	1.839	1.726	1.637	1.468	1.387	1.354
2.00	1.814	1.741	1.656	1.586	1.445	1.368	1.339
2.20	1.711	1.662	1.596	1.541	1.423	1.350	1.325
2.40	1.629	1.597	1.546	1.502	1.403	1.334	1.312
2.60	1.562	1.542	1.502	1.468	1.383	1.319	1.298
2.80	1.506	1.495	1.464	1.437	1.364	1.304	1.286
3.00	1.459	1.454	1.431	1.410	1.346	1.290	1.274
3.20	1.418	1.419	1.402	1.385	1.329	1.277	1.261
3.40	1.384	1.388	1.376	1.363	1.313	1.265	1.249
3.60	1.353	1.361	1.353	1.343	1.299	1.254	1.239
3.80	1.327	1.337	1.332	1.325	1.285	1.243	1.229
4.00	1.303	1.315	1.312	1.309	1.272	1.234	1.220
4.20	1.282	1.295	1.295	1.294	1.260	1.225	1.212
4.40	1.263	1.277	1.279	1.280	1.249	1.217	1.204
4.60	1.246	1.261	1.265	1.267	1.239	1.210	1.198
4.80	1.231	1.246	1.251	1.255	1.231	1.204	1.192
5.00	1.217	1.232	1.239	1.244	1.223	1.198	1.187
5.20	1.204	1.220	1.228	1.234	1.216	1.194	1.183
5.40	1.193	1.208	1.217	1.224	1.210	1.190	1.180
5.60	1.182	1.197	1.207	1.215	1.205	1.187	1.177
5.80	1.172	1.187	1.198	1.207	1.201	1.185	1.175
6.00	1.163	1.178	1.189	1.199	1.199	1.184	1.174

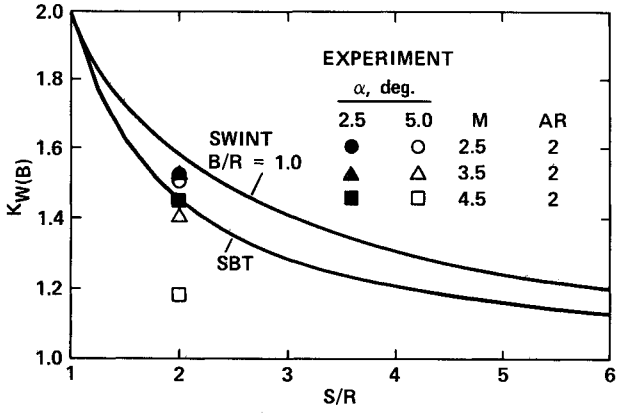

Fig. 10 Comparison of SWINT $K_{W(B)}$ with experiment (from Nielsen, Ref. 27) and slender-body theory.

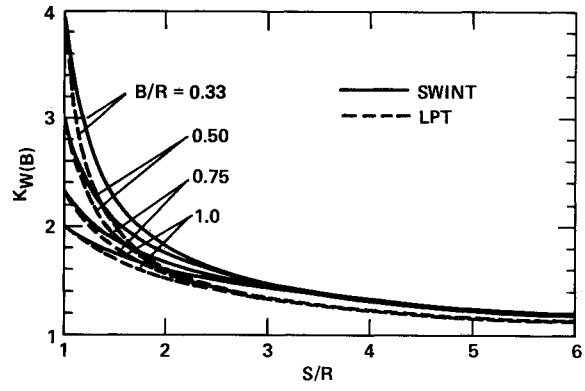

Fig. 12 Comparison of SWINT $K_{W(B)}$ with linearized potential theory for $AR = 3.2$ and $B/R = 0.33$, 0.50, 0.75, and 1.0.

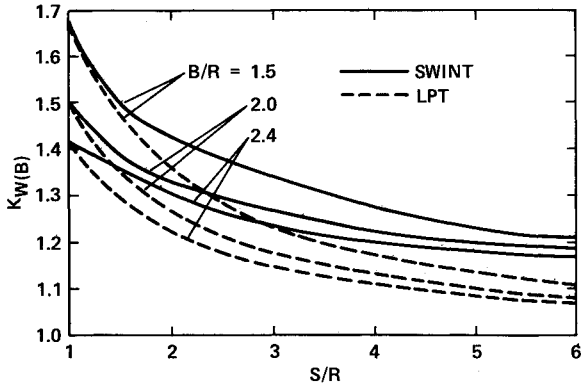

Fig. 11 Comparison of SWINT $K_{W(B)}$ with linearized potential theory at Mach 4 for $AR = 3.2$ and $B/R = 1.5$, 2.0, and 2.4.

shape. Also, the experimental fins had a diamond cross section, whereas the numerical data was generated for infinitely thin fins.

Comparison with LPT

Figures 11 and 12 present a comparison of the present Euler-equation predictions for $K_{W(B)}$ with those from the simple panel upwash, linearized potential theory (LPT).[29] Figure 11 shows $K_{W(B)}$ as a function of S/R for B/R equal to 1.5, 2.0, and 2.4 at Mach 4. Recall that the SWINT data for these B/R ratios changes slightly with Mach number. The LPT data is insensitive to Mach number. SWINT predicts larger values of $K_{W(B)}$ over the entire range of S/R than LPT does.

Figure 12 shows the comparison of $K_{W(B)}$ from SWINT and LPT as a function of S/R for an aspect ratio of 3.2 and for $B/R = 0.33$, 0.50, 0.75, and 1.0. For these values of B/R, both SWINT and LPT data are insensitive to Mach number. The SWINT data shown in Fig. 12 is the average $K_{W(B)}$ as presented in Fig. 9. Again the SWINT predictions yield larger values of $K_{W(B)}$ than the LPT predictions for all values of S/R. The SWINT predictions are more accurate than the LPT results; however, they are much more time consuming to generate.

Table A1 $K_{W(B)}$ equation coefficients

B/R	x_o	C	D	E	F	G	H
0.33	0.60	0.92557	1.24550	1.06140	2.65320	−4.51320	5.86030
0.50	0.60	0.91144	1.56700	0.18539	1.66770	−0.95393	2.28620
0.75	0.60	0.92921	1.61330	−0.32122	1.18140	0.77270	0.37925
1.00	0.60	0.95261	1.58280	−0.63301	1.17220	0.85089	−0.02309
1.50	1.80	2.21060	−0.70822	0.16432	1.71860	−0.16165	0.01250
2.00	2.00	1.72110	−0.26547	0.04436	1.58570	−0.13009	0.01052
2.40	3.00	1.50590	−0.09524	0.00593	1.55030	−0.12237	0.00995

Conclusions

SWINT, a finite-difference Euler code, has been used to determine the effects of elliptical cross-section bodies on the wing lift of supersonic, delta-wing missiles at small angles of attack. Wing-body interference effects on missile lift were correlated in terms of the interference factor $K_{W(B)}$ for elliptical fuselage cross sections with height-to-width ratios $B/R = 0.33$, 0.50, 0.75, 1.0, 1.5, 2.0, and 2.4 for wing span to fuselage-width ratios, $1 \le S/R \le 6$. SWINT $K_{W(B)}$ results were forced to agree with potential theory in the limit of vanishing small fins, because numerical accuracy could not be maintained as S/R approached 1. Values of $K_{W(B)}$ compared well with both slender-body theory results for $1 \le S/R \le 6$ and experimental values at specific values of S/R. The $K_{W(B)}$ results presented herein are amply suited for use in preliminary design for correcting and predicting missile fin lift.

In general, $K_{W(B)}$ decreases as both S/R and B/R increase. As S/R becomes large, the effect of the body on the fin lift becomes negligible and $K_{W(B)}$ approaches 1. $K_{W(B)}$ is larger near $S/R = 1$ and decreases at a faster rate with S/R for fuselages with small B/R, than for fuselages with large B/R.

Numerical results at constant Mach number and fin size show that $K_{W(B)}$ decreases as B/R increases. In general for small fins, typical of missiles, wing lift is very sensitive to fuselage shape. For large wings, typical of airplanes, wing lift is not very sensitive to fuselage shape.

The change of $K_{W(B)}$ with both aspect ratio and Mach number was small over the range of parameters studied, so $K_{W(B)}$ was averaged. This results in one curve of $K_{W(B)}$ vs S/R for each value of B/R, which is independent of aspect ratio, Mach number, and angle of attack, and which is suitable for preliminary design.

$K_{W(B)}$ is an important parameter in the equivalent angle-of-attack method, and it is easy to use in preliminary design to predict resultant lift on the wings in the influence of the body. $K_{W(B)}$ values presented herein are valid at small angles of attack. More extensive research needs to be undertaken to determine the influence of the crossflow shockwaves and vorticity on $K_{W(B)}$ at larger angles of attack.

Appendix: Preliminary Design Equations for $K_{W(B)}$

The SWINT $K_{W(B)}$ data was curve fit as a function of S/R for $1 \le S/R \le 6$ for use in preliminary design. The data for $B/R > 1$ was fit as $K_{W(B)}$ vs S/R. The data for $B/R \le 1$ was fit as $K_{W(B)}$ vs $1/(S/R)$. $K_{W(B)}$ for each B/R case was fit separately in two S/R intervals to minimize error. The slope and magnitude of the two equations were required to be equal at the boundary point x_o, between the two equations. The equations were also required to go through the data point at $S/R = 6$ and to match the linearized potential solution at $S/R = 1$. In all cases, the error between the data points and the final equations was less than 1%.

The curve fit equations are:

$B/R \le 1.0$:

$$K_{W(B)} = C + Dx + Ex^2, \qquad 1/6 \le x \le x_o \qquad \text{(A1a)}$$

$$K_{W(B)} = F + Gx + Hx^2, \qquad x_o \le x \le 1 \qquad \text{(A1b)}$$

where $x = 1/(S/R)$.

$B/R > 1.0$:

$$K_{W(B)} = C + Dx + Ex^2, \qquad 1 \le x \le x_o \qquad \text{(A2a)}$$

$$K_{W(B)} = F + Gx + Hx^2, \qquad x_o \le x \le 6 \qquad \text{(A2b)}$$

where $x = S/R$.

Table A1 gives the values of the coefficients C, D, E, F, G, and H as well as the value of x_o.

Acknowledgment

This work was supported by McDonnell Douglas Astronautics Company, St. Louis, Missouri, through the Independent Research and Development program, monitored by John E. Williams. Additional funds were provided by the Missouri Research Assistance Act. The author acknowledges the contribution of Mr. Christopher Walker for his help with the numerical calculations.

References

[1]Pitts, W. C., Nielsen, J. N., and Kaattari, G. E., "Lift and Center of Pressure of Wing-Body-Tail Combinations at Subsonic, Transonic, and Supersonic Speeds," NASA Rept. 1370, 1957.

[2]Nielsen, J. N., "Supersonic Wing-Body Interference at High Angles of Attack with Emphasis on Low Aspect Ratios," AIAA Paper 86-0568, Jan. 1986.

[3]Ferrari, C., "Interference Between Wing and Body at Supersonic Speeds—Theory and Numerical Application," *Journal of Aeronautical Sciences*, Vol. 15, June 1948, pp. 317–336.

[4]Morikawa, G., "Supersonic Wing-Body Lift," *Journal of Aeronautical Sciences*, Vol. 18, April 1951, pp. 217–228.

[5]Nielsen, J. N., *Missile Aerodynamics,* McGraw-Hill, New York, 1960, pp. 113–143.

[6]Nielsen, J. N. and Pitts, W. C., "Wing-Body Interference at Supersonic Speeds with an Application to Combinations with Rectangular Wings," NACA TN-2677, 1952.

[7]Lomax, H. and Byrd, P. F., "Theoretical Aerodynamic Characteristics of a Family of Slender Wing-Tail-Body Combinations," NACA TN-2554, 1951.

[8]Jaquett, B. M. and Fletcher, H. S., "Experimental Steady-State Yawing Derivatives of a 60-deg Delta-Wing Model as Affected by Changes in Vertical Position of the Wing and in Ratio of Fuselage Diameter to Wing Span," NACA TN-3843, 1956.

[9]Wardlaw, A. B., Baltakis, J. P., and Solomon, J. M., "Supersonic Inviscid Flowfield Computations of Missile Type Bodies," *AIAA Journal*, Vol. 19, July 1981, pp. 899–906.

[10]Priolo, F. J. and Wardlaw, A. B., "A Comparison of Inviscid Computational Methods for Supersonic Tactical Missiles," AIAA Paper 87-0113, 1987.

[11]Jenn, A. A., "Numerical Determination of Missile Aerodynamic Interference Factors," Master's Thesis, Dept. of Mechanical and Aerospace Engineering, Univ. of Missouri—Rolla, Rolla, MO, Dec. 1987.

[12]Jenn, A. A. and Nelson, H. F., "Sideslip Effects on Fin–Fin Interference in Supersonic Missile Aerodynamics," *Journal of Spacecraft and Rockets*, Vol. 25, Nov.–Dec. 1988, pp. 382–392.

[13]Allen, J. M. and Pittman, J. L., "Analysis of Surface Pressure Distributions on Two Elliptic Missile Bodies," *Journal of Spacecraft and Rockets*, Vol. 21, Nov.–Dec. 1984, pp. 528–533.

[14]Amidon, P. F., "Supersonic Aerodynamic Characteristics of Elliptic Cross Section Bodies," AIAA Paper 85-1607, July 1985.

[15]Allen, J. M. and Townsend, J. C., "Application of a Supersonic Euler Code (SWINT) to Wing-Body-Tail Geometries," *Journal of Aircraft*, Vol. 23, June 1986, pp. 513–519.

[16]Priolo, F. J. and Wardlaw, A. B., "Supersonic Noncircular Missile Computations," AIAA Paper 88-0278, Jan. 1988.

[17]Wardlaw, A. B., Hackerman, L. B., and Baltakis, F. P., "An Inviscid Computational Method for Supersonic Missile Type Bodies—Program Description and Users Guide," Naval Surface Weapons Center, White Oak, MD, TR 81-459, Dec. 1981.

[18]Hemsch, M. J. and Nielsen, J. N., "Equivalent Angle-of-Attack Method for Estimating Nonlinear Aerodynamics of Missile Fins," *Journal of Spacecraft and Rockets*, Vol. 20, July–Aug. 1983, pp. 356–362.

[19]Nielsen, J. N., "Nonlinearities in Missile Aerodynamics," AIAA Paper 78-20, Jan. 1978.

[20]Hemsch, M. J. and Nielsen, J. N., "Extension of Equivalent Angle-of-Attack Method for Nonlinear Flowfields," *Journal of Spacecraft and Rockets*, Vol. 22, May–June 1985, pp. 304–308.

[21]Stoy, S. L. and Vukelich, S. R., "Extension of the Equivalent Angle of Attack Prediction Method," AIAA Paper 84-0311, Jan 1984.

[22]Vukelich, S. R., "Aerodynamic Prediction of Elliptically Shaped Missile Configurations Using Component-Buildup Methodology," AIAA Paper 85-0271, Jan. 1985.

[23]Vukelich, S. R., "Development Feasibility of Missile Datcom," Air Force Wright Aeronautics Lab., Wright-Patterson AFB, OH, AFWAL-TR-81-3130, Oct. 1981.

[24]Panton, R. L., *Incompressible Flow*, Wiley, New York, 1984, Chap. 18.

[25]Hughes, W. F. and Brighton, J. A., *Schaum's Outline Series of Fluid Dynamics*, McGraw-Hill, New York, 1967, Chap. 6.

[26]Lamb, Sir Horance, *Hydrodynamics*, Dover Publications, New York, 1945, Chap. 4.

[27]Nielsen, J. N., "Supersonic Wing-Body Interference at High Angles of Attack with Emphasis on Low Aspect Ratios," AIAA Paper 86-0568, Jan. 1986.

[28]Jones, R. A., NASA Langley Research Center, Hampton, VA, private communication, July 1987.

[29]Jenn, A. A. and Nelson, H. F., "Effect of Wing Vertical Position on Lift for Supersonic Delta-Wing Missile Configurations," *Proceedings of the Atmospheric Flight Mechanics Conference*, AIAA, New York, 1988.